DOI: 10.1002/ejic.200500943

An Electron Microscopy Study of New Chemically Twinned Phases in the MgS-Yb_2S_3 System

Esteban Urones-Garrote,*[a] Adrián Gómez-Herrero,[b] Ángel R. Landa-Cánovas,[c] and L. Carlos Otero-Díaz[a,b]

Keywords: Chemical twinning / Electron microscopy / Rare earths / Sulfides / Solid-state structures

Four new phases in the MgS-Yb_2S_3 system have been identified and characterised by means of transmission electron microscopy and associated techniques, such as microdiffraction and X-ray energy dispersive spectroscopy analysis. The observed stoichiometries are: $MgYb_2S_4$ [a = 0.3752(2), b = 1.259(1), c = 1.268(2) nm] and $Mg_2Yb_6S_{11}$ [a = 0.37297(4), b = 1.2592(2), c = 3.4853(3) nm] with orthorhombic symmetry (space group $Cmcm$) and $Mg_3Yb_8S_{15}$ [a = 1.2637(1), b = 0.37176(5), c = 2.4132(2) nm; β = 100.40(1)°] and $MgYb_4S_7$ [a = 1.2578(2), b = 0.3735(3), c = 1.1417(7) nm; β = 104.88(6)°] with monoclinic symmetry (space group $C2/m$). Their structures can be described and derived from the NaCl-type by the crystallographic operation of chemical twinning at the unit-cell level along the $\{113\}_{NaCl}$ planes. The a and b lattice parameters are common in all the structures while the c parameter depends on the total extension of the twin slabs' sequence, n, such that $c \approx n \times d(113)_{MgS}$ (for orthorhombic phases) or $d(001) \approx n \times d(113)_{MgS}$ (for monoclinic phases). All the unit-cell parameters were refined from the X-ray powder diffraction data after the unit-cell symmetries had been deduced from electron microscopy data.

Introduction

The crystallographic operation termed "chemical twinning at the unit-cell level" by Hyde and Andersson[1,2] is very useful for understanding, describing and clarifying many crystal structures as this concept allows the building of apparently complex structures from simple units. The regular and repeated reflection twinning on the {113} planes of the NaCl-type parent structure produces a series of homologous ordered phases in an important number of systems, including sulfides, sulfo salts and oxides.[1,2] Ferraris et al.[3] denote it as a "lillianite homologous series", after the structure of $Pb_3Bi_2S_6$.[4] The twinning operation generates trigonal prisms in the composition planes perpendicular to $[113]_{NaCl}$ that share their triangular faces. The frequency of these composition (or twin) planes is responsible for the stoichiometry. They are separated by blocks of NaCl-type structure whose thickness and ordering reflect the c unit-cell parameter. The block thickness can be denoted by the number of atom layers parallel to the twin planes.[1] The members of the homologous series present equal a and b crystal parameters while the c parameter varies with the total twin slabs' sequence and is proportional to $d(113)_{NaCl}$.

Several phases derived from the NaCl-type by chemical twinning have been reported in the Pb-Bi-S system, such as natural sulfo salts[3] and synthetic samples,[5,6] including $PbBi_4S_7$, with a Y_5S_7-type structure,[7] which presents a ...(4,3)... twin sequence. Other phases with more complex twin slab sequences have also been found, such as $Pb_2Bi_6S_{11}$ [...(4,4,3,4,4,3)...] and $Pb_3Bi_{10}S_{18}$ [...(4,4,3,4,3,4,4,3,4,3)...]. Bakker and Hyde were the first to study these structures by means of transmission electron microscopy (TEM), especially several phases in the Mn-Y-S system,[8] including the phase MnY_2S_4, which has a $CaTi_2O_4$-type structure[9] with a ...(4,4)... twin sequence. Some other phases were observed and predicted between MnY_2S_4 and MnY_4S_7 stoichiometries, such as $Mn_3Y_8S_{15}$ and $Mn_2Y_6S_{11}$, whose structure can be considered as an ordered intergrowth between the former phases.

The Cr-Er-S system has been extensively studied, mainly by X-ray powder diffraction (XRPD) data, by Tomas et al.,[10–12] who reported several different phases, such as $CrEr_2S_4$, $Cr_2Er_6S_{11}$ and $CrEr_4S_7$. The structure of $CrEr_2S_4$ is reported to be a twofold superstructure of MnY_2S_4 along the short axis due to the Jahn–Teller effect on Cr^{2+}-centred octahedra. The $Cr_2Er_6S_{11}$ phase presents the orthorhombic space group $Cmc2_1$, whereas some other phases with the same stoichiometry present the $Cmcm$ space group, including $Fe_2Yb_6S_{11}$[13] and the binary sulfide Tm_8S_{11}.[14] Phases derived from an NaCl-type structure by the operation of

[a] Dpto. Química Inorgánica, Fac. CC. Químicas, Universidad Complutense,
28040, Madrid, Spain
[b] Centro de Microscopía, Universidad Complutense,
28040, Madrid, Spain
[c] Inst. Ciencia de Materiales de Madrid, CSIC,
28049, Madrid, Spain
E-mail: esteban@brunilda.sme.ucm.es

chemical twinning have also been found in the Mn-Er-S series. For example, Tomas et al. have studied the $Mn_{0.4}Er_{4.6}S_7$ phase[15] from single-crystal X-ray diffraction data, and a more detailed characterisation of the system was carried out by TEM.[16,17] Disordered intergrowths of $Mn_2Er_6S_{11}$ and $Mn_3Er_8S_{15}$ along the *c* axis of the structures were also found, along with well-ordered crystals. The transformation of the $MnEr_2S_4$ sulfospinel into different chemically twinned (CT) phases and into NaCl-type structure was observed in this system[18] due to irradiation damage effects under the electron microscope beam (intermediate acceleration voltage of 400 kV). The Ca-Tl-O system presents several CT phases belonging to the homologous series $Ca_nTl_2O_{n+3}$.[19,20] The structure of each phase was further studied by means of neutron diffraction by Berastegui et al.[21]

Some other CT phases have the same stoichiometry as $CaTi_2O_4$ but with a twin sequence that is different to ...(4,4)..., as is the case of $HgBi_2S_4$[22] and $CdBi_2S_4$,[23] which are monoclinic phases with a ...(5,3)... twin slabs' sequence, denoted as a pavonite homologous series by Ferraris et al.[3]

The formation of NaCl-type MS-RE_2S_3 solid solutions (M = divalent metal; RE = rare-earth element) is well documented,[24] mainly by characterisation with XRPD data. When M = Mg, Mn and Ca extensive solid solutions with NaCl-type structure are generated for the heavy rare-earth elements and for Y. Some orthorhombic and monoclinic phases have also been reported in these systems from XRPD data,[25,26] although none was isolated with M = Mg and RE = Yb. TEM studies carried out in the Mg-Yb-S system[27] indicate that a transition from an NaCl-type to a spinel-type structure occurs through short-range order phenomena and segregation of extended defects. In this work, we present the preparation and characterisation of four new CT phases derived from the NaCl-type structure in this ternary system, as determined by TEM and associated techniques [microdiffraction and X-ray energy dispersive spectroscopy (XEDS) analysis]. XRPD information is employed to refine the crystal parameters of each phase once their unit-cell symmetries have been determined from the electron diffraction data.

Results and Discussion

The XRPD patterns of each sample are complex, with a large number of maxima (about 40) in the range $5° \leq 2\theta \leq 70°$ due to the presence of different phases with large unit cells. The diffraction maxima are also broad, which indicates the existence of defects. All these observations were confirmed by the study of the samples by TEM and associated techniques. The phases present in each of the samples were first identified from their selected-area electron diffraction (SAED) patterns, from which the approximate unit-cell dimensions can be obtained and then refined from XRPD data. Four CT ordered phases were observed, with the average stoichiometries indicated in Table 1 and discussed below.

$MgYb_2S_4$

The XRPD pattern indicates the presence of the cubic spinel-type phase $MgYb_2S_4$ [a = 1.0951(2) nm], which has been described previously,[27] as well as other phases. An ordered major phase was identified by means of TEM observations. An orthorhombic unit cell could be assigned to these crystals from SAED patterns taken along different orientations (see Figure 1). The approximate crystal parameters are: $a \approx 0.37$, $b \approx 1.25$, $c \approx 1.26$ nm.

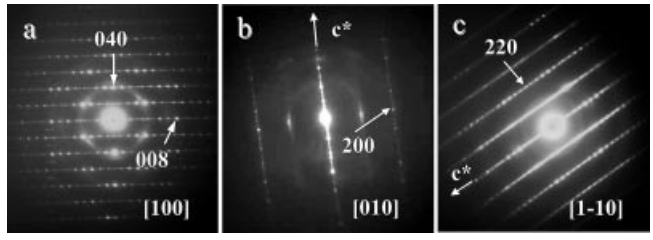

Figure 1. SAED patterns along different orientations, belonging to three different crystals of the sample with a nominal Mg:Yb ratio of 1:2. Note the streaking of the reflections along *c**, which is indicative of the presence of plane defects and/or disorder perpendicular to *c*.

The one-dimensional (1D) intensity streaking of the diffraction maxima along *c** in some of the diffraction patterns indicates the presence of disordered planar defects perpendicular to *c*. The cation ratio was semi-quantitatively measured by XEDS (ten crystals were analysed) with an average result of Mg/Yb = 0.46 [$Mg_{0.93(4)}Yb_{2.03(4)}S_4$], which is very close to a 1:2 stoichiometry. There are several possible orthorhombic structure-types with a similar AB_2S_4 ideal stoichiometry, such as the $CaFe_2O_4$ type[7] (a = 0.9230, b = 0.3024, c = 1.0705 nm; space group *Pnma*), the $CaTi_2O_4$ type[9] (a = 0.3136, b = 0.9727, c = 0.9976 nm; space group *Cmcm*) and the Yb_3S_4 type[28] (a = 1.2777, b = 0.3837,

Table 1. Crystal parameters of the different CT phases previously described, refined from XRPD data. The space group and the twin slabs' sequences inside the unit cell are included in each case.

Phase	XEDS analysis	S/(Mg+Yb) ratio	Space group	Lattice parameters [nm]	Z	Twin sequence
$MgYb_2S_4$	$Mg_{0.93(4)}Yb_{2.03(4)}S_4$	1.333	*Cmcm*	a = 0.3752(2), b = 1.259(1), c = 1.268(2)	4	(4,4)
$Mg_3Yb_8S_{15}$	$Mg_{3.04(9)}Yb_{7.97(6)}S_{15}$	1.363	*C*2/*m*	a = 1.2637(1), b = 0.37176(5), c = 2.4132(2); β = 100.40(1)°	2	(4,4,4,3)
$Mg_2Yb_6S_{11}$	$Mg_{1.96(7)}Yb_{6.03(5)}S_{11}$	1.375	*Cmcm*	a = 0.37297(4), b = 1.2592(2), c = 3.4853(3)	4	(4,4,3,4,4,3)
$MgYb_4S_7$	$Mg_{1.03(6)}Yb_{3.98(4)}S_7$	1.400	*C*2/*m*	a = 1.2578(2), b = 0.3735(3), c = 1.1417(7); β = 104.88(6)°	2	(4,3)

c = 1.2926 nm; space group *Pnma*). The measured unit-cell parameters do not allow us to differentiate between them. The actual space group can be identified by means of the microdiffraction technique[29,30] by studying the "ideal symmetry" of the microdiffraction patterns, which is determined by the position and relative intensity of the reflections, either on the zero-order Laue zone (ZOLZ) or in the whole pattern (WP), which includes high-order Laue zones (HOLZ). The difference of periodicity and the shifts between the Laue zones give information about the presence of glide planes and screw axes and about the centring of the lattice, respectively. A microdiffraction pattern along the [010] zone axis, where a shift of the FOLZ and the ZOLZ along c^* can be observed, is shown in Figure 2 (a). The $h0l$ reflections with $h = 2n + 1$ are absent in the ZOLZ but the $h1l$ ones with $h = 2n + 1$ are present in the FOLZ (first-order Laue zone). Furthermore, $00l$ ($l = 2n + 1$) reflections are observed in the ZOLZ but the $01l$ reflections are absent in the FOLZ. This shift of the Laue zones along c^* due to the indicated extinctions is indicative of the C-centring of the lattice, according to the extinction condition hkl: $h + k = 2n + 1$. Two possible orthorhombic space groups have the same extinction conditions for compounds with the stoichiometry AB_2S_4: *Cmcm* and $Cmc2_1$. The tilted pattern of Figure 2 (b) shows the presence of an *m*-plane perpendicular to *c*, and the [110] ZOLZ microdiffraction pattern of Figure 2 (c) shows (2*mm*) "ideal" symmetry, which confirms, together with the information obtained from the other patterns, that this phase presents the *Cmcm* space group.[29,30] The $Cmc2_1$ space group would have shown (*m*) "ideal" symmetry along the [110] zone axis. Therefore, the major well-ordered phase found in this sample [XEDS: $Mg_{0.93(4)}Yb_{2.03(4)}S_4$] can be considered to be isostructural with a $CaTi_2O_4$-type structure, in other words it can be described as a ...(4,4)... CT structure according to the nomenclature proposed by Hyde and Andersson.[1] An idealised model of this CT-$MgYb_2S_4$ structure, viewed along the [100] direction, is included in Figure 3. Mg^{2+} cations are located in octahedral coordination sites and the Yb^{3+} cations lie in the remaining octahedral sites (50%) and in the bicapped trigonal prisms present in the twin planes. Both cations occur randomly in the octahedral sites.

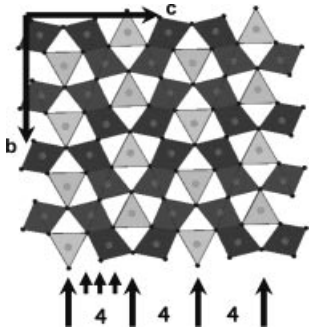

Figure 3. Idealized model of the ...(4,4)... CT structure of the $MgYb_2S_4$ phase (Z = 4). The $\{(Mg,Yb)S_6\}$ octahedra are represented in dark grey and the $\{YbS_{6+2}\}$ bicapped trigonal prisms are represented in light grey. The caps have been excluded from the model for clarity. The twin slabs' sequence in the unit cell is clearly visible.

In order to confirm the proposed structure model, HRTEM (high-resolution TEM) images were taken along the short axis (in this case the *a* axis), which best reflects the CT structure. Figure 4 shows an HRTEM Fourier-filtered image of the CT-$MgYb_2S_4$ phase along [100], and the corresponding fast Fourier transform (FFT) is included as an inset. Simulated images were obtained at several microscope defocus and crystal thickness values, using the ideal $CaTi_2O_4$-type atomic positions and the experimentally refined crystal parameters from XRPD patterns. The best fit with

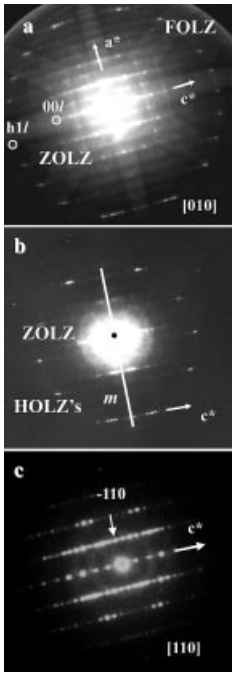

Figure 2. Microdiffraction patterns corresponding to a crystal with a Mg:Yb ratio of 1:2. Information about the centring of the lattice (C) and the actual space group (*Cmcm*) are deduced from them (see the text for details). The pattern in (b) is tilted off-axis in order to observe the HOLZ reflections.

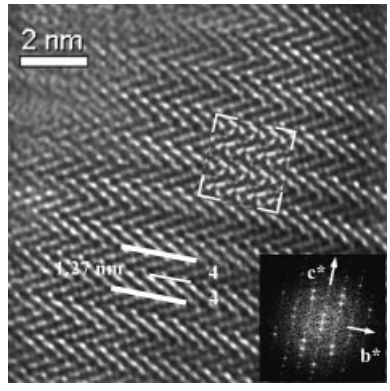

Figure 4. Fourier-filtered HRTEM image of an $MgYb_2S_4$ crystal taken along the short-axis of the CT structure. The corresponding FFT is included in the lower right part as an inset. The simulated image (defocus, Δf = –40 nm; thickness, t = 8 nm) agrees well with the experimental one.

the experimental image is superimposed in Figure 4 and shows a good correspondence with the experimental image, which indicates that the observed phase presents the Ca-Ti_2O_4-type structure.[9]

$MgYb_4S_7$

Detailed TEM observations of the sample with a nominal Mg/Yb ratio of 1:4 showed the existence of a major, well-ordered phase as well as a minor $MgYb_2S_4$ spinel phase (which was not observed in the XRPD pattern) and crystals with disordered lattice planes. The SAED patterns of the major phase (see Figure 5) can be assigned to a monoclinic phase with the approximate unit cell parameters $a \approx 1.26$, $b \approx 0.37$ and $c \approx 1.15$ nm, and $\beta \approx 105°$.

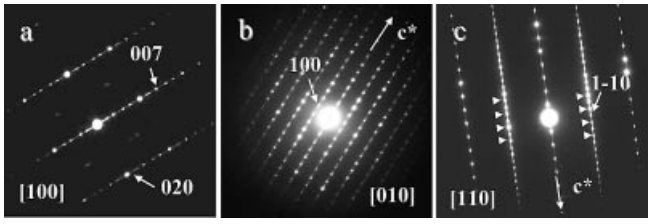

Figure 5. SAED patterns along different orientations, belonging to different crystals of the sample with a nominal Mg:Yb ratio of 1:4. Note the intensity streaking of the reflections along c^*, which is indicative of the presence of defects and/or disorder.

XEDS analyses of 10 crystals provided the average cation ratio Mg/Yb $\approx$ 0.26 [$Mg_{1.03(6)}Yb_{3.98(4)}S_7$], which is very close to 1:4 ratio. A possible structure type with AB_4S_7 stoichiometry is Y_5S_7,[7] whose structure can be described as a ...(4,3)... CT phase.

The actual space group can be identified by means of microdiffraction patterns. Thus, the [100] microdiffraction pattern of Figure 6 (a) shows that the ZOLZ reflections are shifted by $1/2\,b^*$ with respect to the FOLZ ones. The $0kl$ reflections turn into $1kl$ reflections in the FOLZ, and are absent when $1 + k = 2n + 1$. The shift provoked by these extinctions is indicative of the C-centring of the lattice. The [110] ZOLZ microdiffraction pattern in Figure 6 (b) presents (*2*) "ideal" symmetry, which agrees with the *C*2/*m* space group,[29,30] whereas *C*2 and *Cm* space groups, which present the same extinction conditions, would display (*1*) "ideal" symmetry along the same zone axis. Therefore, microdiffraction results support the *C*2/*m* space group rather than *C*2 or *Cm*, and the observed phase can be described as a ..(4,3)... CT phase, with an ideal $MgYb_4S_7$ stoichiometry [XEDS: $Mg_{1.03(6)}Yb_{3.98(4)}S_7$] and a Y_5S_7-type structure.

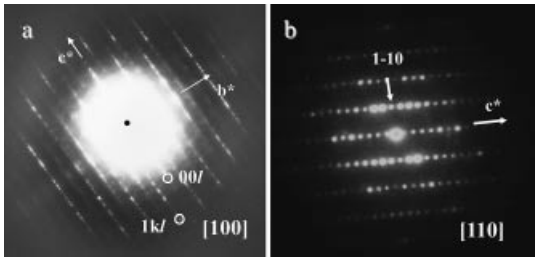

Figure 6. Microdiffraction patterns corresponding to the major ordered phase in the sample with a nominal Mg:Yb ratio of 1:4. The C-centring of the lattice is deduced from (a) and the "ideal" symmetry of the ZOLZ pattern in (b) − (*2*) − indicates that the phase presents the *C*2/*m* space group. See text for details.

Note that some intensity streaking is observed in the diffraction maxima along c^* in the SAED patterns of Figure 5, which is indicative of plane defects perpendicular to *c*. Furthermore, in the [110] SAED pattern of Figure 5 (c), extra maxima are present (marked with arrows) due to the presence of macroscopic twin planes in the crystal, parallel to (001), which can be attributed to unit-cell twin sequences of the type ...4,3,4,3,4/4,3,4,3,4...

An idealised model of the CT-$MgYb_4S_7$ structure, along [010], is shown in Figure 7, where Mg^{2+} and half of the Yb^{3+} cations lie in octahedral sites at random and the other half of the Yb^{3+} cations lie in the trigonal prisms at the composition planes.

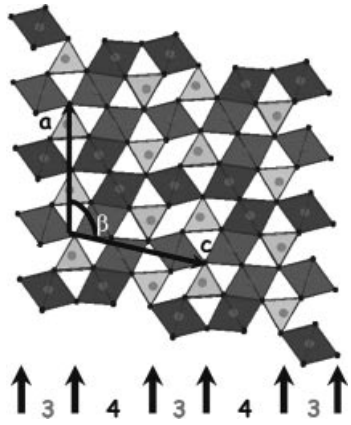

Figure 7. Idealized model of the ...(4,3)... CT structure of the $MgYb_4S_7$ phase (isostructural with Y_5S_7). The {(Mg,Yb)S_6} octahedra are represented in dark grey, and the {YbS_6} trigonal prisms are represented in light grey.

HRTEM images were obtained along the short axis of the structure to confirm the proposed model. Image simulations were calculated from the ideal atomic positions of the Y_5S_7-type structure and the refined crystal parameters from the XRPD pattern. The correspondence of the experimental images and the simulated ones is quite good, as shown in Figure 8, thus confirming the proposed structure model.

$Mg_3Yb_8S_{15}$ and $Mg_2Yb_6S_{11}$ Phases

TEM observations from the crystals previously described as $MgYb_2S_4$ and $MgYb_4S_7$ showed the existence of disorder along c^* due to the presence of both phases intergrown in a disordered manner. The ordered crystals found in this system had 3:8 and 1:3 Mg/Yb ratios, so two new samples were prepared with these nominal chemical compositions.

In the first case the XEDS analyses of ten crystals indicated a Mg/Yb ratio of about 0.38, close to an ideal $A_3B_8S_{15}$ stoichiometry [$Mg_{3.04(9)}Yb_{7.97(6)}S_{15}$], as reported before in the Mn-Er-S system[16,17] mentioned above. This phase is monoclinic, with the following approximate lattice

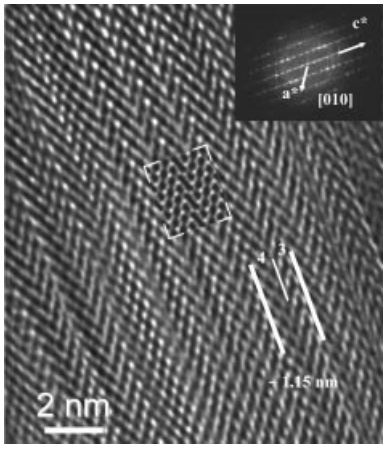

Figure 8. Fourier-filtered HRTEM image along the short axis of a CT-$MgYb_4S_7$ crystal ([010] direction). The corresponding FFT is included as an inset. The simulated image (Δf = –50 nm; t = 2 nm) agrees well with the experimental one.

parameters measured from SAED patterns (see Figure 9): $a \approx 1.26$, $b \approx 0.37$, $c \approx 2.40$ nm; $\beta \approx 100°$.

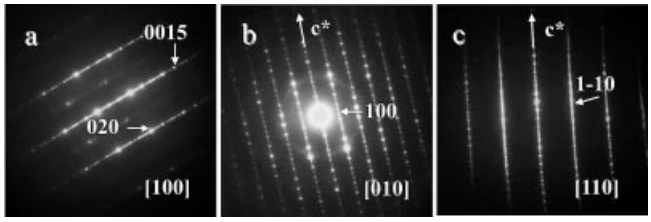

Figure 9. SAED patterns along different orientations, belonging to different crystals of the sample with a nominal Mg:Yb ratio of 3:8.

Most of the observed CT-$Mg_3Yb_8S_{15}$ crystals present streaking along c*, so the identification of its actual space group by means of microdiffraction patterns was problematic. However, the C-centring of the lattice was observed in the [100] microdiffraction pattern due to the shift of the ZOLZ and FOLZ reflections.

HRTEM images along the short axis of the structure (see Figure 10) indicated a ...(4,4,4,3)... twin slabs' sequence. The simulated image that showed the best fit among different defocus and thickness values is shown as the inset in Figure 10. The calculations were performed with the ideal atomic positions directly obtained from the ...(4,4,4,3)... model and the HRTEM image (*C*2/*m* space group), and with the crystal parameters refined from XRPD data. Therefore, according to this model, the CT-$Mg_3Yb_8S_{15}$ structure presents a ...(4,4,4,3)... twin sequence, with Mg^{2+} and half of the Yb^{3+} cations in octahedra (at random) and the other half in trigonal prisms at the composition planes (see Figure 11).

In the case of the sample with a 1:3 cation ratio, the previously described CT phases were observed, together with the sulfospinel $MgYb_2S_4$. An orthorhombic ordered phase was also found, with the following approximate crystal parameters obtained from SAED patterns: $a \approx 0.37$, $b \approx 1.26$, $c \approx 3.50$ nm.

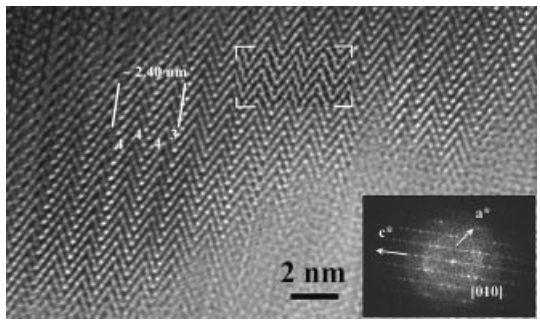

Figure 10. Fourier-filtered HRTEM image along the short axis of a CT-$Mg_3Yb_8S_{15}$ crystal ([010] direction). The corresponding FFT is included as an inset. The simulated image (Δf = –50 nm; t = 2 nm) agrees well with the experimental one. It was calculated by employing the preliminary crystal parameters measured from SAED patterns (*C*2/*m* space group) and the atomic parameters directly obtained from the ideal model and from the image.

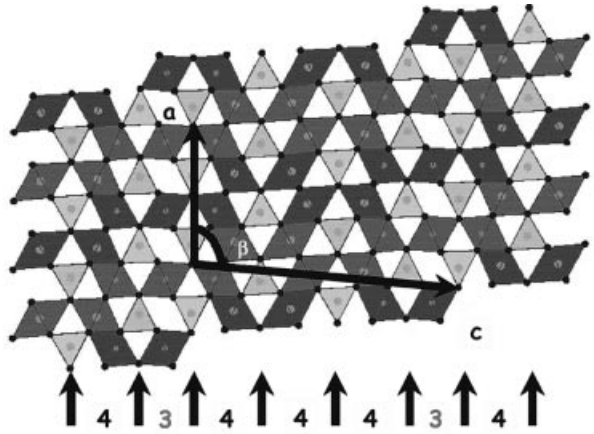

Figure 11. Idealized model of the CT-$Mg_3Yb_8S_{15}$ phase (Z = 2). The twin slabs' sequence is ...(4,4,4,3)... in this case. The {(Mg,Yb)-S_6} octahedra are represented in dark grey, and the {YbS_6} trigonal prisms are represented in light grey.

The measured XEDS (six crystals) Mg/Yb ratio was about 0.32, which corresponds to a 1:3 cation stoichiometry. The chemical composition and lattice parameters are similar to the previously described Tm_8S_{11} and $Mn_2Er_6S_{11}$ structures,[14,17] so that the average XEDS analysis can be formulated as $Mg_{1.96(7)}Yb_{6.03(5)}S_{11}$. The crystals belonging to this CT phase are usually disordered along c* (1D intensity streaking of the diffraction spots along that direction, as observed in the SAED patterns; see Figure 12). The model was confirmed by HRTEM images, such as the one shown in Figure 13 along the [110] orientation. The experimental image agrees quite well with the simulated one (inset) calculated with the ideal $Fe_2Yb_6S_{11}$ atomic positions (*Cmcm* space group) and with the crystal parameters refined from the XRPD data. Therefore, the observed $Mg_2Yb_6S_{11}$ structure is a new phase and can be described as a ...(4,4,3,4,4,3)... CT one. As in the previously described phases, Mg^{2+} and half of the Yb^{3+} cations occupy octahedral positions at random, whereas the other half of the Yb^{3+} cations lie in the trigonal prisms at the composition planes, as shown in the structural model in Figure 14.

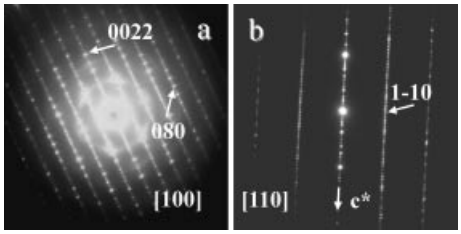

Figure 12. SAED patterns along different crystal orientations, belonging to the sample with a nominal Mg:Yb ratio of 1:3. Intensity streaking along the c^* reflections can be observed due to the presence of plane defects perpendicular to c.

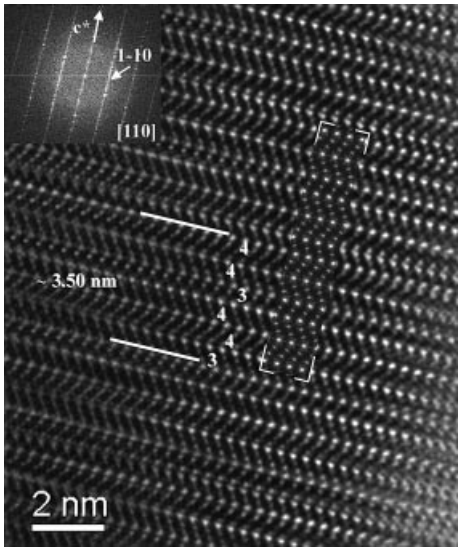

Figure 13. Fourier-filtered HRTEM image of the CT-$Mg_2Yb_6S_{11}$ phase along the [110] direction. The corresponding FFT is included as an inset. The simulated image (Δf = –50 nm; t = 6 nm) agrees well with the experimental one and reflects the twin slabs' sequence in the unit cell.

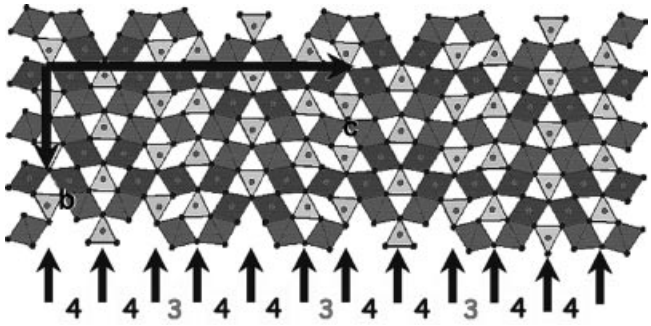

Figure 14. Idealized model of the ...(4,4,3,4,4,3)... structure of the CT-$Mg_2Yb_6S_{11}$ phase. It presents the $Fe_2Yb_6S_{11}$-type structure (*Cmcm* space group and Z = 4). The {(Mg,Yb)S_6} octahedra are represented in dark grey, and the {YbS_{6+1}} mono-capped trigonal prisms are represented in light grey (the caps have been excluded for clarity).

Disorder perpendicular to c is common in these phases, as was previously observed in the SAED patterns (1D streaking). Intergrowths were also found in many crystals, as can be seen in the HRTEM image included in Figure 15, where slabs of $Mg_2Yb_6S_{11}$ and $Mg_3Yb_8S_{15}$ alternate along c, apparently at random.

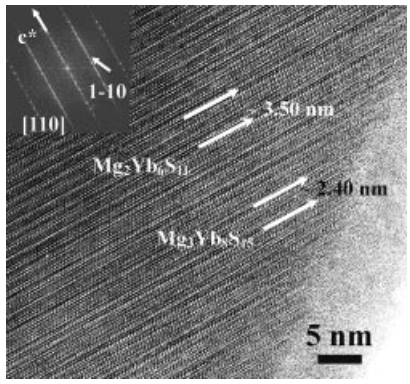

Figure 15. HRTEM image of a crystal from the sample with nominal composition $Mg_2Yb_6S_{11}$, showing a disordered intergrowth of the CT-$Mg_3Yb_8S_{15}$ and CT-$Mg_2Yb_6S_{11}$ structures along c. The corresponding FFT is included as an inset.

In the phases derived from the NaCl-type structure by chemical twinning the c parameter accounts for the twin blocks periodicity [$c \approx n \times d(113)_{MgS}$ for orthorhombic phases and $d(001) \approx n \times d(113)_{MgS}$ for monoclinic ones], i.e., it indicates the stoichiometry of the phase. The value of n, which stands for the total extension of the NaCl-type slabs between the twin planes included in the unit cell, can be derived from the superstructure periodicity along $[113]^*_{NaCl}$ (or c^*). Figure 16 includes an enlargement of the c^* rows belonging to the four CT phases described in this work, with n = 8 for CT-$MgYb_2S_4$, n = 15 for CT-$Mg_3Yb_8S_{15}$, n = 22 for CT-$Mg_2Yb_6S_{11}$ and n = 7 for CT-$MgYb_4S_7$ (see Table 1).

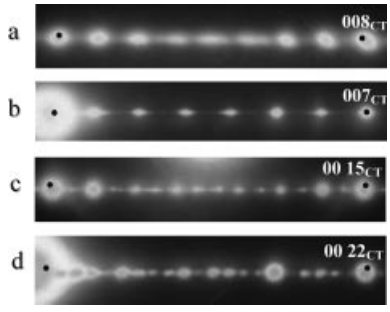

Figure 16. Detail of the 00l reflections row (c^*) of the four CT phases described in this work. The superstructure periodicity inside 113_{NaCl} is directly related to the twinning sequence (n). a) $MgYb_2S_4$, with n = 8 and twin sequence ...(4,4)...; b) $MgYb_4S_7$, n = 7 and ...(4,3)...; c) $Mg_3Yb_8S_{15}$, n = 15 and ...(4,4,4,3)...; d) $Mg_2Yb_6S_{11}$, n = 22 and ...(4,4,3,4,4,3)...

XRPD Studies

Once the four observed phases had been identified and characterised by means of TEM and associated techniques, the lattice parameters were refined from XRPD data. The results are summarised in Table 1, including the twin slabs' sequences.

Since the origin of these CT structures is the regular and repeated twinning on $\{113\}_{NaCl}$ planes, the variation of $d(113)_{NaCl}$ vs. composition has been studied in the MgS-Yb_2S_3 system, including samples with NaCl and spinel structures reported previously,[27] with lower Yb^{3+} content than the CT phases described in this work. The change in $d(113)_{NaCl}$ with the Yb/Mg ratio is represented in Figure 17. This parameter increases in the NaCl-type structure samples as the Yb^{3+} concentration is increased, since the ionic radius of Yb^{3+} in sixfold coordination (0.1008 nm) is bigger than in the case of Mg^{2+} (0.0710 nm).[31] The introduction of Yb^{3+} into the matrix of MgS generates cation vacancies.[27] When a spinel-type phase is formed with higher Yb^{3+} content, there is a sudden variation in $d(113)_{NaCl}$ [$\approx 1/2 \times d(113)_{spinel}$], which is related to the structure change, with ordering of vacancies. It remains constant with slight composition variations since the unit-cell enlargement due to the increase of vacancies and Mg^{2+} substitution by Yb^{3+} must be compensated by the occupancy of tetrahedral positions.[27] When considering the CT phases described in this work, the $d(113)_{NaCl}$ value, which is directly related to the $d(001)_{CT}$, as mentioned before, decreases significantly and abruptly with respect to the spinel phase values due to the elimination of all the cation vacancies by the chemical twinning operation. The $d(113)_{NaCl}$ value decreases slightly (see Figure 17) as the relative number of composition planes in the unit cell of each CT phase increases, i.e., from $MgYb_2S_4$ [two composition planes every eight $(113)_{NaCl}$ planes] to $MgYb_4S_7$ [two composition planes every seven $(113)_{NaCl}$ planes].

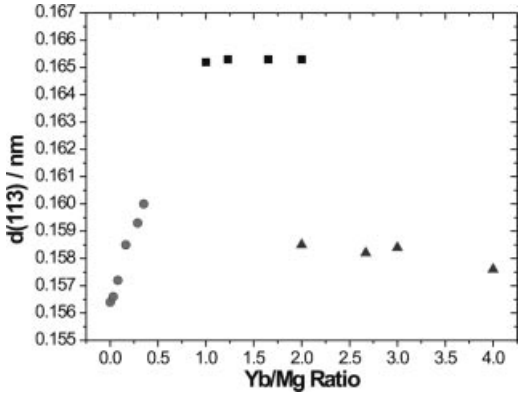

Figure 17. Variation of $d(113)_{NaCl}$ with the Yb/Mg ratio. The grey circles correspond to phases with an NaCl structure,[27] the black squares correspond to phases with a spinel-type structure with cationic excess[27] and the grey triangles correspond to the CTP phases described in this work.

Conclusions

As can be observed in Table 1, the phases described in this work present common *a* and *b* crystal parameters while the *c* axis changes according to the composition. It was mentioned previously that the composition variations in the phases derived from the NaCl-type structure by the chemical twinning operation are accommodated through the twin slabs' sequence and periodicity, i.e., the generation of twin (composition) planes. These CT structures can be considered as members of a homologous series, with the two different symmetries (orthorhombic and monoclinic) depending on the twin slabs' sequence within the unit cell and with variation of the *c* axis with the stoichiometry.

As the twin sequence gets more complicated, i.e. the *c* axis gets larger, the difficulty of long-range ordering increases, as was observed in the $Mg_3Yb_8S_{15}$ and $Mg_2Yb_6S_{11}$ phases, which very often present intergrowths between CT structures. These two phases, whose Mg/Yb ratio lies between $MgYb_2S_4$ and $MgYb_4S_7$, are regular intergrowths of the ...(4,4)... and the ...(4,3)... sequences. Therefore, within this composition range, some other ordered phases could be expected, as predicted by Bakker et al.[8] in the Mn-Y-S system or as observed in other related systems,[5,11,13,14] which are actually built up from the $MgYb_2S_4$ and $MgYb_4S_7$ "units". In the system studied in this work, no more ordered CT phases were observed.

The co-existence of the CT-$MgYb_2S_4$ and the normal spinel with the same nominal stoichiometry is an interesting case of polymorphism, which extends to the high-pressure polymorph with Th_3P_4-type structure.[32] We have not been able to relate this polymorphism with temperature (annealing at 1373 K does not give any change in the relative abundance of the phases). However, slight but significant composition differences have been found between them, as measured by XEDS analysis. The CT-$MgYb_2S_4$ phase presents an excess of Yb^{3+} with respect to the Mg/Yb ratio of 0.50, while the spinel phase has an excess of Mg^{2+} [XEDS: $Mg_{1.1(1)}Yb_{1.92(7)}S_4$]. Therefore, although the AB_2S_4 composition is the ideal one for both phases, it seems to be the separating line between them.

Experimental Section

Preparation of the Samples: Several mixtures of nitrates $Mg(NO_3)_2 \cdot 6H_2O$ and $Yb(NO_3)_3 \cdot 5H_2O$ were placed in graphite boats inside a tubular furnace and heated under a flow of H_2S (10%)/Ar (50 mL/min) and Ar (20 mL/min) (bubbling in CS_2). The samples with nominal cation ratio (Mg/Yb) 1:2 and 1:4 were prepared at 1273 K for 10 h, whereas the other ones (3:8 and 1:3) were treated first at 798 K for 4 h and then at 1273 K for four more hours. The gas flow was maintained while raising the temperature. Each sample was cooled down to room temperature by switching off the furnace and maintaining a flow of Ar to avoid oxidation. The gases at the exit of the furnace were neutralised in a concentrated NaOH solution.

Characterisation of the Samples: Specimens for TEM observations were obtained from suspensions ultrasonically dispersed in butanol. A drop of each corresponding suspension was placed on a copper grid covered with a holey carbon film. A JEM 2000FX electron microscope, equipped with a LINK ISIS 300 XEDS analysis system, was employed to explore the reciprocal lattice of the samples (double-tilt specimen holder: ±45°) and to analyse the chemical composition. A Philips CM200 FEG (field emission gun) electron microscope, equipped with an EDAX DX4 XEDS analysis system was employed for the microdiffraction studies. HRTEM images were taken with a JEM 3000F (point resolution: 0.17 nm)

electron microscope. Due to the preferential cleavage of the crystals, the short axis of the structures under study could not be observed because they were beyond the tilt capacities of the JEM 3000F microscope (double-tilt specimen holder: ±20°). Therefore, the samples were embedded in epoxy resin and thin slices were obtained with an ultramicrotome for TEM observations. Crystals close to the short-axis orientation could be found in this way.

The as-prepared sulfides were studied by XRPD, using a Philips X'pert Diffractometer (Cu-$K_{\alpha 1}$ radiation) to refine the lattice parameters.

Acknowledgements

The authors acknowledge the financial support from the MCYT to the project with reference MAT2003-08465-C02-01.

[1] S. Andersson, B. G. Hyde, *J. Solid State Chem.* **1974**, *9*, 92–101.
[2] B. G. Hyde, S. Andersson, M. Bakker, C. M. Plug, M. O'Keeffe, *Prog. Solid State Chem.* **1979**, *12*, 273–327.
[3] G. Ferraris, E. Makovicky, S. Merlino, *Crystallography of Modular Materials*, Oxford University Press, Oxford, **2004**.
[4] J. Takagi, Y. Takéuchi, *Acta Crystallogr., Sect. B* **1972**, *28*, 649–651.
[5] D. Colaïtis, D. Van Dyck, S. Amelinckx, *Phys. Status Solidi A* **1981**, *68*, 419–438.
[6] A. Prodan, M. Bakker, M. Versteegh, B. G. Hyde, *Phys. Chem. Miner.* **1982**, *8*, 188–192.
[7] B. G. Hyde, S. Andersson, *Inorganic Crystal Structures*, Wiley, New York, **1989**.
[8] M. Bakker, B. G. Hyde, *Philos. Mag. A* **1978**, *38*, 615–628.
[9] E. F. Bertaut, P. Blum, *Acta Crystallogr.* **1956**, *9*, 121–126.
[10] A. Tomas, R. Chevalier, P. Laruelle, B. Bachet, *Acta Crystallogr., Sect. B* **1976**, *32*, 3287–3289.
[11] A. Tomas, J. Rigoult, M. Guittard, P. Laruelle, *Acta Crystallogr., Sect. B* **1980**, *36*, 1987–1989.
[12] A. Tomas, M. Guittard, *Mater. Res. Bull.* **1980**, *15*, 1547–1556.
[13] S. M. Chaqour, A. Tomas, P. Lemoine, *Acta Crystallogr., Sect. C* **1994**, *50*, 1655–1657.
[14] Y. Zhang, H. F. Franzen, B. Harbrecht, *J. Less-Common Met.* **1990**, *166*, 135–140.
[15] A. Tomas, M. Robert, C. Adolphe, M. Guittard, *Mater. Res. Bull.* **1984**, *19*, 1643–1646.
[16] J. Arce de la Plaza, L. C. Otero-Díaz, *J. Less-Common Met.* **1985**, *110*, 371–374.
[17] A. R. Landa-Cánovas, L. C. Otero-Díaz, *Aust. J. Chem.* **1992**, *45*, 1473–1487.
[18] A. R. Landa-Cánovas, L. C. Otero-Díaz, *Solid State Ionics* **1993**, *63–65*, 378–387.
[19] F. Goutenoire, V. Caignaert, M. Hervieu, C. Michel, B. Raveau, *J. Solid State Chem.* **1995**, *114*, 428–435.
[20] F. Goutenoire, V. Caignaert, M. Hervieu, B. Raveau, *J. Solid State Chem.* **1995**, *119*, 134–141.
[21] P. Berastegui, S. Eriksson, S. Hull, F. J. García-García, J. Eriksen, *Solid State Sci.* **2004**, *6*, 433–441.
[22] W. G. Mumme, J. A. Watts, *Acta Crystallogr., Sect. B* **1980**, *36*, 1300–1304.
[23] W. Choe, S. Lee, P. O'Connell, A. Covey, *Chem. Mater.* **1997**, *9*, 2025–2030.
[24] J. Flahaut, in *Handbook on the Physics and Chemistry of Rare Earths*, vol. 4 (Ed.: K. Gschneider, L. Eyring), North Holland, Amsterdam, **1979**, 1.
[25] M. Patrie, J. Flahaut, *C. R. Acad. Sci. Paris* **1967**, *264*, 395–398.
[26] C. Adolphe, P. Laruelle, *Bull. Soc. Fr. Minéral. Cristallogr.* **1968**, *91*, 219–232.
[27] E. Urones-Garrote, A. Gómez-Herrero, A. R. Landa-Cánovas, R. L. Withers, L. C. Otero-Díaz, *Chem. Mater.* **2005**, *17*, 3524–3531.
[28] L. C. Otero-Díaz, A. R. Landa-Cánovas, B. G. Hyde, *J. Solid State Chem.* **1990**, *89*, 237–259.
[29] J. P. Morniroli, J. W. Steeds, *Ultramicroscopy* **1992**, *45*, 219–239.
[30] M. Tanaka, M. Terauchi, *Convergent-Beam Electron Diffraction*, Jeol-Maruzen, Tokyo, **1985**.
[31] R. D. Shannon, *Acta Crystallogr., Sect. A* **1976**, *32*, 751–767.
[32] K. Hirota, N. Kinomura, S. Kume, M. Koizumi, *Mater. Res. Bull.* **1976**, *11*, 227–232.

Received: October 25, 2005
Published Online: February 15, 2006

